ACS Catalysis

Research Article

pubs.acs.org/acscatalysis

Doped Graphene as a Material for Oxygen Reduction Reaction in Hydrogen Fuel Cells: A Computational Study

M. Kaukonen,*[,†] A. V. Krasheninnikov,[‡,§] E. Kauppinen,[†] and R. M. Nieminen[‡]

[†]NanoMaterials Group, Department of Applied Physics and Center for New Materials, Aalto University, P.O. Box 15100, FI- 00076 Aalto, Espoo, Finland

[‡]COMP/Applied Physics, Aalto University, P.O. Box 1100, FI-00076 Aalto, Finland

[§]Department of Physics, University of Helsinki, P.O. Box 43, FI-00014 Helsinki, Finland

ABSTRACT: Because of its high specific surface area and unique electronic properties, graphene with substitutional impurity metal atoms and clusters attached to defects in the graphene sheet is attractive for use in hydrogen fuel cells for oxygen reduction at the cathode. In an attempt to find a cheap yet efficient catalyst for the reaction, we use density-functional theory calculations to study the structure and properties of transition-metal-vacancy complexes in graphene. We calculate formation energies of the complexes, which are directly related to their stability, along with oxygen and water adsorption energies. In addition to metals, we also consider nonmetal impurities like B, P, and Si, which form strong bonds with under-coordinated carbon atoms at defects in graphene. Our results indicate that single Ni, Pd, Pt, Sn, and P atoms embedded into divacancies in graphene are promising candidates for the use in fuel cell cathodes for oxygen reduction reaction (ORR). We further discuss how ion irradiation of graphene combined with metal sputtering and codeposition can be used to make an efficient and relatively inexpensive graphene-based material for hydrogen fuel cells.

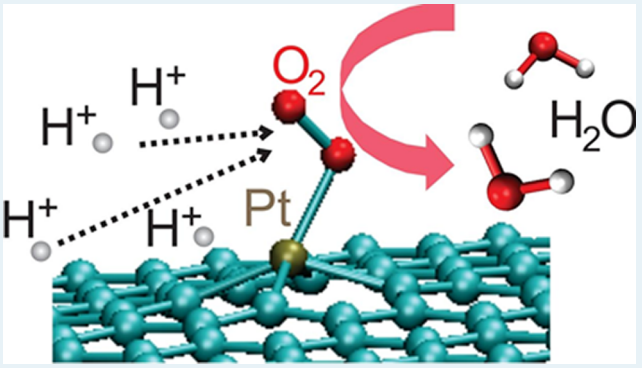

KEYWORDS: *graphene, DFT, oxygen reduction reaction, irradiation, impurity, vacancy*

1. INTRODUCTION

Fuel cells (FCs),[1] ecologically friendly devices which directly convert chemical energy into electricity with high efficiency, are one of the most promising developments for future energy solutions. Currently their main usages are to function as reliable power sources when a long-time endurance is needed or to power transport applications. Among FCs of various designs, proton exchange membrane FCs[2] with hydrogen fuel have received considerable attention because of they offer a good compromise between output power, working temperature/pressure ranges, weight, and efficiency. The main challenges to be overcome are related to fuel storage (storage of H_2), the endurance of the FC and its efficiency, which is currently in the range of 30−50%, considerably lower than, for example, in magnesium-air or direct-carbon FCs (80−90%).[3]

The main energy losses in low temperature FCs are related to excessively high energy barriers at cathodes, which slow down the reaction kinetics and give rise to heating. In the ideal cathode reaction (cathode is the electrode where water is formed by hydrogen oxidation) the initial oxygen binding to the cathode material should be nearly reversible because this reaction does not drive electrons in the power loop.[4] The subsequent reaction steps of adding protons with electrons to the system should ideally be isoenergetic to avoid energy loss as heat.[5−7] At the moment, the best cathode materials are made of Pt and other expensive substances, and finding a cheaper catalyst is one of the major challenges for the FC industry.[8−10] The adsorption energy of O_2 on platinum surfaces has been calculated as ≈ −70 kJ/mol, and the height of the subsequent energy barriers toward water formation have been estimated of the order of 10−20 kJ/mol.[11] On the other hand, larger energy barriers have been obtained by Morais and co-workers: 10−80 kJ/mol.[12]

Since its isolation in 2004,[13] graphene has extensively been studied in the context of future energy solutions because of its unique electronic and mechanical properties and extremely high surface area. Specifically, this two-dimensional (2D) one-atom-thick material has been demonstrated to be promising for hydrogen[14] and electricity[15] storage, as well as for energy harvesting from the environment.[16] It has also been considered for use in FCs as support for the catalyst[17]at both anodes[18] (the electrode at which, in case of hydrogen FC, hydrogen molecules are split into protons and electrons) and cathodes.[19] Graphene doped with nitrogen[20] or sulfur[17] has been investigated for ORR. As defects in graphene provide good anchoring for small metal clusters[18,21] and even for isolated

Received: September 14, 2012
Revised: December 9, 2012

   dx.doi.org/10.1021/cs300605t | ACS Catal. 2013, 3, 159−165

atoms,[22,23] graphene-metal systems have been widely studied in this context.[24−26] Nevertheless, the efficiency of graphene-based FCs should be improved considerably, and more important, their cost reduced, before such FCs become commercially viable.

First-principles computational methods have proven to be extremely successful in a rational design of solid catalysts.[27] In this article we employ density-functional theory (DFT) calculations to study the feasibility of graphene with impurities for operation in cathodes of FCs. We focus on the oxygen adsorption reaction at the cathode and try to find materials which have low binding energy for oxygen. We further consider another issue: the formation energy of the cathode material, which should be as low as possible to warrant high stability of the system. We demonstrate that single Ni, Pd, Pt, Sn, and P atoms embedded into divacancies in graphene can be promising candidates for the use in FC cathodes for ORR. We further discuss how ion irradiation of graphene combined with metal sputtering and codeposition can be used to make an efficient and relatively inexpensive graphene-based material for hydrogen FCs.

2. RESULTS

We focused our computational analysis on calculations of the formation energies of impurity complexes composed from vacancies in graphene with adsorbed impurity atoms and evaluation of the adsorption energies of the O_2 molecule on the complexes. In terms of the stability, the formation energy of the defect should be as low as possible; on the other hand, the adsorption energy should be negative (exothermic reaction) to facilitate binding, but the absolute value should not be too large, as strong binding can hinder the later reaction steps.

The formation energy $E^f(n_A,n_B,n_V)$ of a defect complex containing n_A atoms of the impurity species A, n_B atoms of the impurity species B, with respect to a graphene sheet with missing n_V carbon atoms is calculated as

$$E^f(n_A, n_B, n_V) = E^{tot}(n_A, n_B, n_V) - n_C\mu_G - n_A\mu_A - n_B\mu_B \quad (1)$$

where E^{tot} is the total energy of the system, and μ_G, μ_A, and μ_B are the chemical potentials of the carbon atom in graphene and those of atoms A and B in the reference bulk structures, respectively. The numbers of impurities in the defect (n_A, n_B) range from zero to two in this study and $n_C = n_{tot} - n_V$, where n_{tot} is the total number of carbon atoms in the ideal graphene plane (here n_{tot} = 98). In eq 1 it is assumed that either a vacancy or a divacancy is present in the sample, so that the formation energy of the defect is not included. We stress that although the concentration of vacancies in thermodynamic equilibrium in graphene is negligible even at elevated temperatures because of high formation energies of these defects (7−8 eV),[28] vacancies in this material can be formed due to ion or electron irradiation.[29,30] The reference bulk structure is the hexagonal closed packed structure (space group (SG) 194) for Co, Ru, Sc, Ti, and Zn; cubic close packed (SG225) for Ag, Al, Cu, Ni, Pd, Pt, Rh; body centered cubic for Cr, and V (SG229). For As and Bi SG166 is used, for P we use black phosphorus (SG64), for Ga SG62, and for Mn alpha-Mn (SG217). The initial structures for the bulk systems are obtained from the American Mineralogist database.[31]

The initial geometries for the single impurity at a mono- or divacancy were such that the impurity atom was within the graphene plane with equal distances to its three or four nearest carbon neighbors, Figure 1. For the double impurity at a double-vacancy, the two impurity atoms were either on one side of the graphene plane (1 Å away from the plane) or on different sides of the plane. When calculating oxygen adsorption energy, we started geometry optimization with O_2 bound to the impurity atom in either a vertical or a horizontal fashion with respect to the graphene plane.

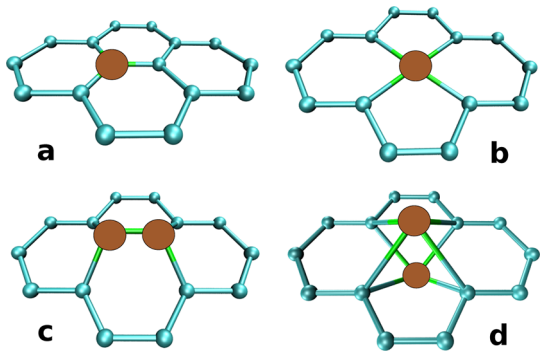

Figure 1. Initial geometries for impurity atom(s) at a mono- or divacancy on graphene. Small blue spheres represent nearby C atoms, while blue brown spheres stand for the impurity atoms. The single impurity atom was positioned initially at the center of a mono- or divacancy (a and b in the figure, respectively). The two impurity atoms were initially placed either on one side, 1 Å above the graphene plane (c in the figure) or on the opposite sides of the graphene plane at the center of the divacancy (d in the figure).

The adsorption energy, $E^a(O_2)$, of O_2 molecule on impurity complexes in graphene is calculated as

$$E^a(O_2) = E^{tot}(n_M n_V O_2) - E^{tot}(n_M n_V) - E^{tot}(O_2) \quad (2)$$

Here $E^{tot}(n_M n_V O_2)$ is the total energy of the system when O_2 has been adsorbed on the surface and $E^{tot}(O_2)$ is the total energy of O_2 molecule in vacuum. We assume that in either formation or adsorption energy the changes in zero point energies, entropy contributions, and solvation effects are small as compared to the changes in the enthalpies, and thus they are neglected in this study. Furthermore, their contributions may partially cancel as we discuss below. The absolute value of entropy component of the free energy of the O_2 molecule in water is of the order 20 kJ/mol (0.2 eV) at room temperature, and the change in the zero point energy upon binding is less than 0.1 eV.[32−34] Recently, the polarization effect by surrounding water is calculated to be of the order of 0.4 eV favoring the bound oxygen molecule on platinum surface.[35] Experimentally, the change in the entropy component of the free energy (the $-TS$ term) in binding of O_2 to iron or cobalt structures is typically 0.1−0.4 eV at room temperature favoring the unbound state.[36] On the basis of the above, in our zero temperature calculations we considered zero energy as the optimal value for the calculated adsorption energy of O_2, eq 2. We stress that a small shift in this value (by 0.1−0.2 eV) does not change any conclusions of this study.

2.1. Impurity Atom at a Single Vacancy (SI@SV). The single impurity at the single vacancy (SI@SV) has three carbon neighbors with equal impurity atom-carbon bonds, except for Ag and Zn which also have three carbon neighbors, but the bond lengths differ (Table 1). Additionally, the impurity atom is displaced 1.3−1.9 Å from the graphene plane, except for Ag, Bi, and Sn (elevations 2.1−2.4 Å). Upon binding of O_2 the

dx.doi.org/10.1021/cs300605t | ACS Catal. 2013, 3, 159−165

Table 1. Lowest Energy Geometries of a Oxygen-Free/Oxygen-Bound Single Impurity/Single Vacancy Complexes (SI@SV/O_2@SI@SV) or at a Double Vacancy (SI@SV/O_2@SI@SV) or at a Double Impurity at a Double Vacancy (DI@DV/O_2@DI@DV)[a]

Imp.	SI@SV	SI@DV	DI@DV	Imp.	SI@SV	SI@DV	DI@DV
Sc	3/12h0	4/4h0	A/A	Ti	3/3ht	4/4ht	A/B
V	3/21ht	4/4h0	A/D	Cr	3/21ht	4/4h0	E/E
Mn	3/21ht	4/4h0	A/B	Fe	3/21ht	4/4h0	A/B
Ru	3/21ht	4/4h0	B/B	Co	3/3h0	4/4h0	C/B
Rh	3/3ht	4/4h0	C/E	Ni	3/3hs	4/4ht	C/D
Pd	3/3hs	4/4ht	C/C	Pt	3/3ht	4/4ht	C/C
Cu	3/21hs	4/nb	C/D	Ag	12/21hs	4/nb	D/D
Zn	21/21h0	4/nb	D/nb	B	3p/3ht	4p/coob	3p/B
Al	3/21ht	4/4h0	E/D	Ga	3/3vt	4/4vt	D/D
Si	3/3ht	4/4vt	C/C	Sn	3/nb	4/4vt	A/nb
P	3/3h0	4/4vt	B/B	Bi	3/nb	4/nb	E/E

[a]The entries on the left-hand side refer to a geometry with no oxygen and on the right-hand side to that with a bound O_2. Symbols in the table: "Imp.": impurity, "3", "4": three or four nearest neighbor C atoms with equal bond lengths (within 0.05 Å), "coob": O_2 covalently bound to C and B atoms. The impurities are elevated from the graphene plane, except B which remains in the graphene plane (symbol "p" in the table). "12" stands for an impurity having one short and two long bonds to the C atoms (in "21" vice versa). Five categories for the geometries of two impurity atoms at a di-vacancy are shown in and labeled from A to E (Figure 6). The symbols related to the oxygen-bound structures are depicted in Figure 2, Figure 5 and Figure 7. Finally "nb" indicates that O_2 does not bind.

impurity−carbon bond length increases by ∼0.05−0.1 Å. The impurity−carbon bonds gain length either equally or one bond becomes longer compared to the two other ones. The dioxygen prefers to bind horizontally along the graphene plane instead of a vertical alignment (with the exception of Ga). We observe four possible bonding geometries for O_2 bound at a single impurity atom at a single vacancy (O_2@SI@SV, Figure 2). In three cases (B, Sn, Bi) we were not able to find oxygen binding to the complex. The O_2@SI@SV complex carries a spin magnetic moment which decreases upon oxygen binding for early d-elements and increases for the late ones. For p-elements, the spin magnetic moment is not affected by oxygen binding.

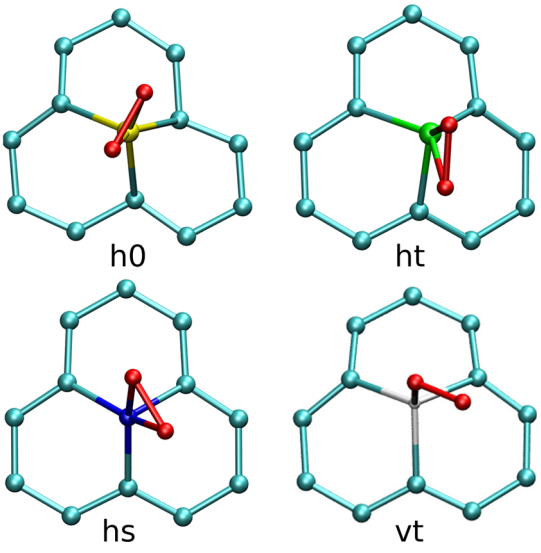

Figure 2. Possible symmetries of the adsorbed O_2 molecule at a single impurity-single vacancy complex (O_2@SI@SV). In the "h0" geometry the O_2 sits in the middle of the defect and both oxygen atoms have the same elevation from the graphene plane. In the "ht" configuration the O−O bond is aligned along one impurity-C bond and the O_2 is slightly tilted with respect to the graphene plane. In the "hs" geometry the O_2 molecule has moved along one bond, and it is perpendicularly aligned with respect to that bond. In the "vt" configuration, only one of the oxygen atoms binds to the impurity.

The formation energies E_f of a single impurity atom to a single vacancy are presented in Figure 3. Additionally, the binding energies of dioxygen to these defects are shown Figure 3. Generally, the binding energy decreases with increasing d-band filling for O_2@SI@SV. It can be understood from the positioning of the mean energy of the metal d-band with respect to oxygen energy levels.[37] All the d-elements show a strong binding with oxygen, with perhaps Zn as an exception (E_{ads} = −0.7), but the formation energy of this complex is high. The only plausible candidate for ORR at a single vacancy is Ga. It has a low formation energy and a reasonable binding energy,

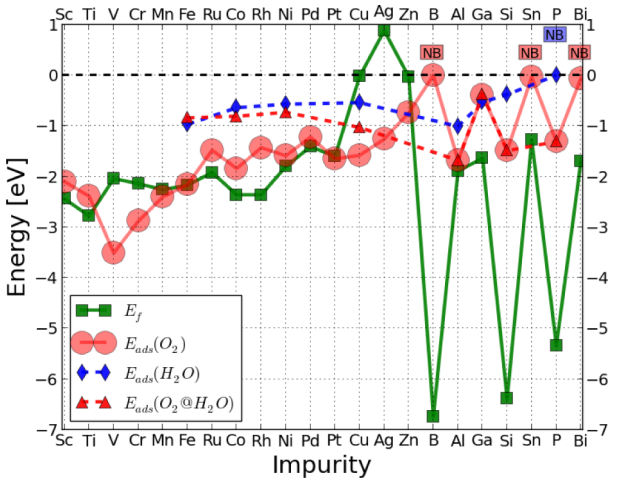

Figure 3. Formation energies, E_f(SI@SV), with respect to bulk chemical potentials for single impurity atoms at a single vacancy on graphene and the adsorption energies of O_2 on that defect, $E_{ads}(O_2)$. Red symbol "NB" stands for "not binding" of O_2 to B, Sn, and Bi. The desired adsorption energy ∼0.0 eV is shown as a horizontal dashed line. Binding energies of water are shown as blue diamonds (P does not bind water, blue "NB" in the figure). Binding energies of dioxygen given that a water molecule has already adsorbed at the defect on the other side of the graphene plane are shown as red triangles.

dx.doi.org/10.1021/cs300605t | ACS Catal. 2013, 3, 159−165

but unfortunately it has a higher affinity to water compared to O_2. These results agree quantitatively with the data by Garcia-Lastra et al. for (6,6) carbon nanotubes.[38]

The observation of a strong binding of O_2 to 3d metals is perhaps a little surprising. It was earlier reported that Ti with its four valence electrons (2× 4s, 2× 3d) forms three σ-bonds and one π-bond to its three carbon neighbors.[22] We find here that upon O_2 binding to Ti, the electrons participating in the Ti−C bonding also participate in the Ti−O bonding. Furthermore, the bonding structure between Ti and its neighbors remains rather intact upon O_2 binding.

As water is formed at the FC cathode, one has also to consider its binding to impurities at the cathode. The adsorption energy of water to selected impurities is shown as blue diamonds, $E_{ads}(H_2O)$, in 2. For the d-elements, binding energy of water is less as compared to oxygen by ∼0.5−1.0 eV. The only exception found here is Ga@SV complex which binds water slightly stronger than oxygen molecules. This may hinder the applicability of Ga@SV for ORR. Water at the P@SV complex does not bind.

Finally, we also considered co-binding. Here O_2 and H_2O are simultaneously bound at the impurity on the opposing sides of the graphene plane. The resulting adsorption energies for adding O_2 to a defect where H_2O is already present are shown as red triangles with dotted lines in Figure 3. The water bound precursor brings the adsorption energy of O_2 on Fe, Co, Ni, and Cu closer to the desired weak chemisorption. However, water seems to prevent dioxygen binding to Ga@SV. For other p-elements studied, O_2 binds more strongly as compared to H_2O and causes the H_2O to desorb. It is unclear whether the co-binding of O_2 and H_2O for d-elements at the single vacancy is possible. This is because the single ligand geometry (with both O_2 and H_2O) is such that the impurity is not on the graphene plane but elevated of the order of 1.3−1.9 Å toward the ligand from the graphene plane possibly causing energy barriers for the binding of a second molecule. The simultaneous binding of two oxygen molecules at the same defects as for co-binding of O_2 and H_2O was also considered, but none of the studied defects was capable on binding two O_2.

2.2. Impurity Atom at a Double Vacancy (SI@DV). The geometries of a single impurity atom at a divacancy (SI@DV) are listed in Table 1. The impurity atom adopts typically a position in the middle of the divacancy slightly elevated from the graphene plane ("4" in the table, elevations of the order of 0.5−1.0 Å). Formation energy of an single impurity, E_f(SI@DV), at the divacancy is lower compared to the single vacancy for late d-metals Pt, Cu, Ag, Zn and for the p-element Al. For Ni the difference in E_f between single and double vacancy is small (0.1 eV preference for SV). Upon oxygen binding the metal atom is elevated from the graphene plane, and for none of the studied impurities it remains on the graphene plane (except for the not-oxygen-binding Cu and Zn). Three categories of geometries of the bound O_2 at SI@DV are shown in Figure 5. As an exception, Boron makes a dramatic geometry change upon oxygen adsorption: it changes from planar midvacancy geometry to nearly substitutional (2 C neighbors), but O_2 binds strongly between B and one carbon next to the divacancy, leaving one dangling bond carbon atom next to the divacancy. For efficient ORR, this O_2 adsorption is far too strong. There are no clear trends in the change of the magnetization for the d-metals, while for the p-elements the oxygen binding increases the magnetization.

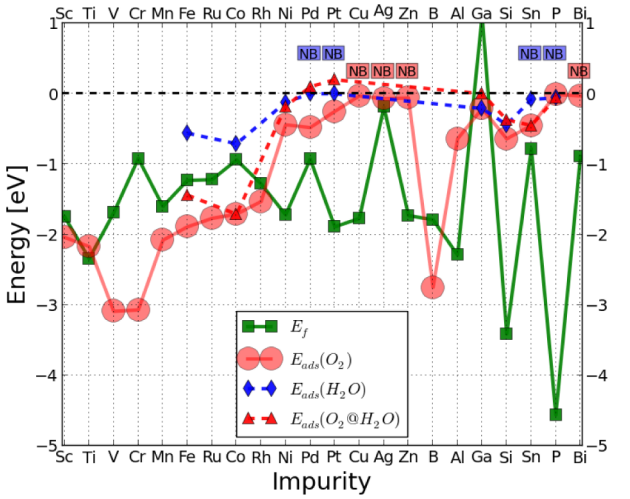

Figure 4. Formation energies, E_f(SI@DV), with respect to bulk chemical potentials for single impurity atoms at a divacancy in graphene and the adsorption energies of O_2 to that defect, $E_{ads}(O_2)$. Red symbol "NB" stands for "not binding" O_2 for Cu, Ag, Zn, and Bi. The desired calculated adsorption energy ∼0.0 eV is shown as a horizontal dashed line. Binding energies of water are shown as blue diamonds (Pd, Pt, Sn, and P do not bind water). The binding energies of dioxygen given that a water molecule has already adsorbed at the defect are shown as red triangles. Pd, Pt, Ga, and P do not bind O_2 given that H_2O is already bound.

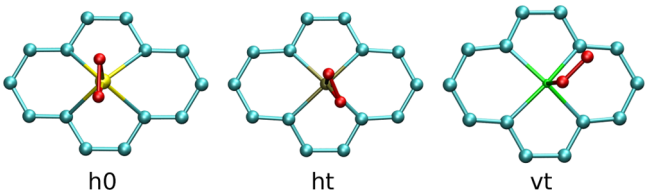

Figure 5. Three possible atomic configurations of the adsorbed O_2 molecule at a single impurity at a double vacancy (O_2@SI@DV complex). In the "h0" geometry O_2 is in the middle of the defect and both oxygen atoms have the same elevation from the graphene plane. In the "ht" configuration the O−O bond is aligned along one impurity-C bond and the O_2 is slightly tilted with respect to the graphene plane. In the "vt" arrangement, only one of the oxygen atoms binds to the impurity.

There are more divacancy-based complexes suitable for ORR as compared to the single vacancy. The best candidates having a mild oxygen binding are late d-metals Ni, Pd, Pt and p-elements Al, Ga, Si, Sn, and P. Nevertheless, the Ga complex appears to have too high a formation energy, and it has again (as in the case of Ga@SV) a higher affinity to water as compared to the dioxygen.

It is instructive to take a closer look at the two cases, namely, Ni and P complexes and to compare O_2 binding to these defects at a single and a double vacancy. In the case of P@SV there is a very good overlap of P and O_2 related orbitals. This is because the nature of the P−C bonding is ionic when oxygen is not bound (Bader analysis indicates P(II)) and thus new P−O bonds can be easily formed without breaking covalent P−C bonds. The result is a large binding energy of O_2, Figure 3. In the case of P@DV the bonding of phosphorus with both C and O remains ionic upon oxygen binding resulting in a low oxygen binding energy, Figure 4. For the Ni@DV the projected density of states indicates that some covalent Ni−C bonding is lost upon O_2 binding thus causing energy penalty for the oxygen

dx.doi.org/10.1021/cs300605t | ACS Catal. 2013, 3, 159−165

binding. On the contrary, the Ni−C bonds at Ni@SV remain rather intact upon O_2 binding, explaining the stronger oxygen binding to Ni@SV compared to Ni@DV.

Similarly to the SI@SV complexes, H_2O is generally bound weaker at SI@DV as compared to O_2, except for Ga for which H_2O replaces O_2. Water does not bind at Ni, Pd, Pt, and P at a double vacancy. Finally, it is found that Pd, Pt, and P can bind two O_2 molecules with a binding energy close to zero (E_b < 0.1 eV).

2.3. Two Impurity Atoms at a Single Divacancy (DI@DV). Two impurity atoms at a divacancy (DI@DV) on graphene adopt most typically a geometry in which metal atoms are bonded to each other but are located on the opposite sides of the graphene plane (70% of the studied impurities, Figure 6

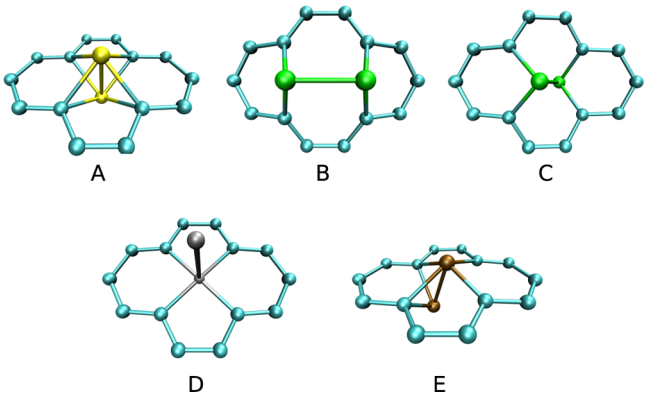

Figure 6. Atomic structures of two impurity atom-at a double vacancy (DI@DV complexes). In the "A" geometry the impurity atoms are located symmetrically on the opposite sides of the graphene plane, each having four nearest carbon neighbors. In the "B" configuration the impurity atoms are on the same side of the graphene plane with two nearest neighbor carbon atoms. In the geometry "C" the impurity atoms are located on the opposite sides of the graphene plane, each having two nearest carbon neighbors. In the "D" configuration one of the impurity atoms is in the middle of the divacancy near the graphene plane, and the other one is loosely bound to the surface. In the configuration "E" impurity atoms are on the opposite sides of the graphene plane, each having 1−4 nearest neighbors.

A). Another rare configuration (Ru_2@DV and P_2@DV) is the horizontal alignment in which the impurity atoms are on the same side of the graphene plane (Figure 6, B). The third configuration is the one where one impurity atom is located at the middle of the divacancy in the graphene plane and the other is out of the plane position with one bond to the mid-divacancy impurity and with 0−2 bonds to carbon (Figure 6,D). In some cases, the impurity atoms are on the opposite sides of the graphene plane, with a varying number of nearest neighbors (Figure 6, C, E).

The formation energies for two-impurity defects at a divacancy involving d-elements are usually higher when compared to single atom impurities, except for early 3d-elements Sc_2 and Ti_2 and most p-elements: B, Ga, Sn, and P (Figure 8). This indicates that there might be a stable configuration of a single impurity atom at a divacancy which could withstand clustering with other impurity atoms.

There are not many promising candidates for the centers for ORR among the double impurities at a divacancy. The only ones possessing the low formation energy combined with the desired weak oxygen affinity are Ga (with the possible problem with a stronger affinity for water), Ag, and P (Figure 3). The

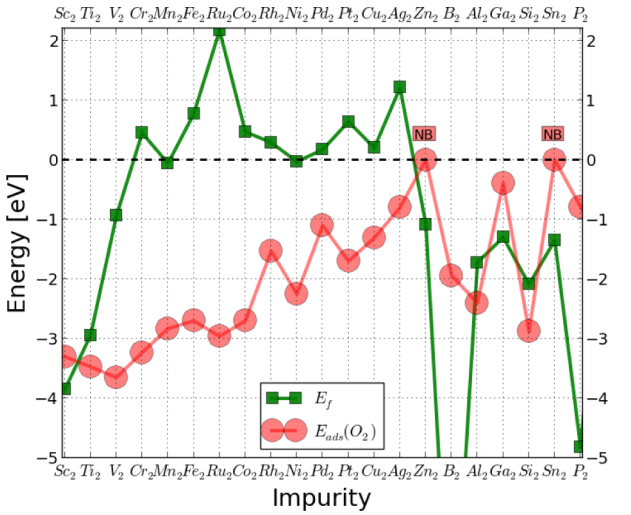

Figure 8. Formation energies (E_f) of two impurity atoms at a divacancy (DI@DV) on graphene and the adsorption energies of $E_{ads}(O_2)$ to that defect. The desired adsorption energy ~0.0 eV is shown as a horizontal dashed line. Red symbol "NB" stands for "not binding" of O_2 to Zn_2 and Sn_2.

rich variety of the configurations of O_2 bound to DI@DV are depicted in Figure 7. Finally, we also studied some heterometal centers at DV, Table 2, but we were not able to find a suitable low binding energy for O_2.

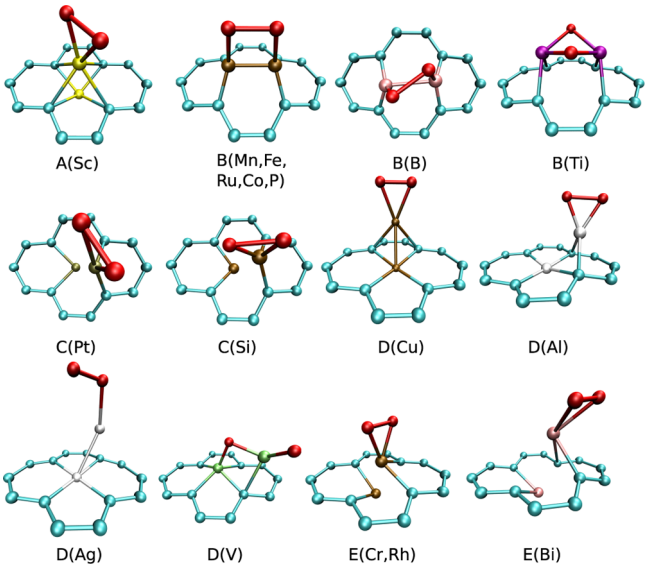

Figure 7. Atomic configurations of O_2 molecules bound to two impurity atoms at a double vacancy. In the nomenclature listed under each configuration the letters (A, B, etc.) stand for DI@DV configuration, Figure 6, while the chemical elements are given in the parentheses.

2.4. Energetics of the Oxygen Reduction Reaction. Up to now we have searched for the best candidates for ORR by calculating the adsorption energy of an oxygen molecule to the defect on the surface. To complete our study, we calculate the energetics of the whole ORR pathway for most promising impurities at divacancies in graphene. The energy of the system composed of graphene slab with impurity and isolated molecules is taken as the zero energy. The intermediates and

dx.doi.org/10.1021/cs300605t | ACS Catal. 2013, 3, 159−165

Table 2. Defect Formation and Oxygen Adsorption Energies for Some of the Configurations Presented in Figure 6[a]

species	E_f	$E_{ads}(O_2)$	geom.
MnZn	−0.9	−2.2	D(Mn)/A(Mn−O_2)
FeCu	0.0	−2.1	D(Fe)/D(Fe)(Fe−O_2)
FeAg	−0.1	−2.0	D(Fe)/D(Fe)(Fe−O_2)
NiCo	0.0	−2.2	D(Ni)/D(Ni)(Co−O_2)
NiBi	−1.1	0.0	D(Ni)/D(Ni)nb
CuBi	−0.7	−2.1	D(Cu)/D(Cu)2BiOC
AgBi	+0.5	−0.8	E/E(Ag−O_2)

[a]The symbols in the table refer to a particular configuration in Figure 6. "nb" means that O_2 does not bind (NiBi).

their energies with respect to unbound O_2 molecule are shown in Table 3 and Figure 9. Al and Si impurities bound water

Table 3. Cumulative Energetics of the Oxygen Reduction Reaction at Selected Single Atom Impurities at a Di-Vacancy in [eV][a]

imp	a	b	c	d/d′	e	f	g
Ni	0.0	−0.4	−0.3	−2.1/−2.3	−3.9	nb	−5.1
Pd	0.0	−0.5	−1.2	−3.2/−2.4	−4.2	nb	−5.1
Pt	0.0	−0.3	−1.0	−3.6/−2.7	−4.6	nb	−5.1
Al	0.0	−0.6	−1.8	−3.8/−2.4	−5.4	−5.7	−5.1
Si	0.0	−0.6	−2.0	−3.7/−3.2	−5.6	−5.6	−5.1
Sn	0.0	−0.6	−1.7	−1.9/−2.6	−5.1	nb	−5.1
P	0.0	0.0	−1.4	−1.7/−3.6	−5.0	nb	−5.1

[a]The symbols (a−g) in the table refer to a particular configuration in Figure 9. The symbol "nb"' means that water is not stable at the defect, but dissociates spontaneously.

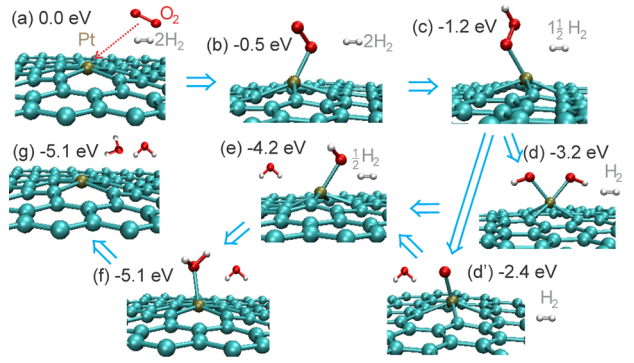

Figure 9. Energetics of the oxygen reduction for O_2@Pd@DV. The cumulative reaction energy from oxygen and hydrogen molecules to water is shown.

rather strongly, and this will likely hinder their applicability for ORR. On the contrary, at Ni, Pd, Pt, Sn, and P impurities water dissociates spontaneously. Also all the reaction steps for Ni, Pd, Pt, Sn, and P are exothermic. Therefore these are our proposed candidates for ORR.

3. CONCLUSIONS AND OUTLOOK

Using first-principles calculations, we have studied the possibility of using various impurity atoms embedded in graphene with defects for oxygen reduction reaction (ORR). A good defect-candidate for ORR should first have a low formation energy to facilitate stability, and second it should bind O_2 weakly (an adsorption energy close to zero) to avoid losses because of unnecessarily high energy barriers at later steps toward water formation.

We calculated the geometry and formation energies of transition-metal-vacancy complexes in graphene along with oxygen and water adsorption energies. In addition to metals, we also considered nonmetal impurities like B, P, and Si, which form strong bonds with under-coordinated carbon atoms at defects in graphene. With regard to the defects, we considered single and double-vacancies. Taking a low formation energy of the complex, which is directly related to its stability, and a weak O_2 binding affinity as the main criteria for a good catalyst, we selected a number of promising complexes. We also calculated the energetics of the whole process, and our results indicate that single Ni, Pd, Pt, Sn, and P atoms embedded into divacancies in graphene can be good candidates for the use in FC cathodes for ORR.

P_2, Ga_2, and Ag_2 can possibly work as a double impurity at a double vacancy for ORR. Some of the double impurities (P_2, Pd_2, and Pt_2) can even bind two O_2 molecules. Zn is the only possible candidate for ORR at a single vacancy among the impurities studied, but it has a rather high formation energy. Ga has the desired low binding affinity to oxygen in all cases (Ga@SV, Ga@DV, Ga_2@DV), but water is able to replace oxygen which may hinder applicability of Ga in the FC applications.

Experimentally, such systems can be created by irradiating graphene with predeposited metal clusters with energetic (1−100 keV) ions. For example, 10 keV Ar ions should create about 0.4 double vacancy per impact,[39] and at the same sputter a considerable amount of impurity atoms from the clusters. As migration energies of ad-atoms on graphene are lower than those for vacancies,[40] the system may be kept at moderate temperatures (ca. 100 °C) during irradiation of the sample at the heating stage, thus offering the best opportunities for pinning of atoms on reactive vacancies. Such an approach has been experimentally shown[41] to be feasible for electron irradiation. Alternatively, impurity atoms can be evaporated in situ onto irradiated graphene from a heated filament.[23] Such a two-step post-irradiation substitutional doping has been proven to be effective for introducing single-atom impurities into graphene.[42] Individual atoms (instead of clusters) should decrease the amount of the catalyst needed and thus reduce the cost of the cells.

4. METHODS

The calculations are carried out using the VASP density functional code (version 5.2).[43,44] We use an energy cutoff of 325 eV for the plane waves to build up the electron wave functions. The geometries are conjugate-gradient relaxed until the maximum force at an atom is less than 0.01 eV/Å. The spin-polarized version of the density functional theory is used. For the analysis of partial charges at atoms we utilize the Bader charge partition scheme.[45] The pseudopotentials made by the projector augmented-wave method are applied.[46] For the p-elements only the s and p electrons are treated as valence electrons, except for Ga and Sn where also the 3d and 4d electrons, respectively, are accounted for. For the 3d elements, the 4s and 3d electrons are treated as valence ones, except for Ti, V, Cr, and Mn for which also the 3p electrons are taken into account. For Sc also the 3s electrons are included as valence electrons. The generalized-gradient approximation is used in the exchange and correlation potential introduced by Perdew et al.[47]

The graphene system in this study consists of 7 × 7 × 1 unit cells (98 atoms). We use 4 × 4 × 1 evenly spaced *k*-points for integration over the Brillouin zone of the supercell. The dimension of the simulation cell to the direction of the graphene surface normal is chosen in such a way that there is at least 10 Å between periodic

dx.doi.org/10.1021/cs300605t | *ACS Catal.* 2013, 3, 159−165

images. When calculating chemical potentials of impurities, lattice constant and energies for the corresponding bulk systems were optimized using a 10 × 10 × 10 *k*-point mesh.

AUTHOR INFORMATION

Corresponding Author

*E-mail: markus.kaukonen@iki.fi.

Notes

The authors declare no competing financial interest.

ACKNOWLEDGMENTS

This research has been supported by MIDE program of Aalto University and by the Academy of Finland. We acknowledge the generous computer resources provided by the Finnish IT Center for Science (CSC) and by Aalto Science-IT project.

REFERENCES

(1) O'Hayre, R.; Cha, S.; Colella, W.; Prinz, F. *Fuel Cell Fundamentals*; Wiley: New York, 2009.
(2) Wee, J.-H. *Renewable Sustainable Energy Rev.* **2007**, *11*, 1720−1738.
(3) *Fuel cell handbook*, 2004; www.netl.doe.gov/technologies/coalpower/fuelcells/seca/pubs/FCHandbook7.
(4) Tian, F.; Anderson, A. B. *J. Phys. Chem. C* **2011**, *115*, 4076−4088.
(5) Nørskov, J.; Rossmeisl, J.; Logadottir, A.; Lindqvist, L.; Kitchin, J.; Bligaard, T.; Jonsson, H. *J. Phys. Chem. B* **2004**, *108*, 17886−17892.
(6) Greeley, J.; Nørskov, J. *J. Phys. Chem. C* **2009**, *113*, 4932−4939.
(7) Kjaergaard, C.; Rossmeisl, J.; Nørskov, J. *Inorg. Chem.* **2010**, *49*, 3567−3572.
(8) Zhong, C.-J.; Luo, J.; Fang, B.; Wanjala, B. N.; Njoki, P. N.; Loukrakpam, R.; Yin, J. *Nanotechnology* **2010**, *21*, 062001.
(9) Paul, S.; Nardelli, M. *Appl. Phys. Lett.* **2010**, *97*, 233108.
(10) Lim, D.-H.; Negreira, A. S.; Wilcox, J. *J. Phys. Chem. C* **2011**, *115*, 8961−8970.
(11) Hyman, M.; Medlin, J. *J. Phys. Chem. B* **2006**, *110*, 15338−15344.
(12) De Morais, R.; Sautet, P.; Loffreda, D.; Franco, A. *Electrochim. Acta* **2011**, *56*, 10842−10856.
(13) Novoselov, K. S.; Geim, A. K.; Morozov, S. V.; Jiang, D.; Zhang, Y.; Dubonos, S. V.; Grigorieva, I. V.; Firsov, A. A. *Science* **2004**, *306*, 666−669.
(14) Subrahmanyam, K. S.; Kumar, P.; Maitra, U.; Govindaraj, A.; Hembram, K. P. S. S. *Proc. Natl. Acad. Sci. U.S.A.* **2011**, *108*, 2674−2677.
(15) Stoller, M. D.; Park, S.; Zhu, Y.; An, J.; Ruoff, R. S. *Nano Lett.* **2008**, *8*, 3498−3502.
(16) López-Suárez, M.; Rurali, R.; Gammaitoni, L.; Abadal, G. *Phys. Rev. B* **2011**, *84*, 161401.
(17) Liang, Y.; Li, Y.; Wang, H.; Zhou, J.; Wang, J.; Regier, T.; Dai, H. *Nat. Mater.* **2011**, *10*, 780−786.
(18) Zhou, Y.-G.; Chen, J.-J.; bin Wang, F.; Sheng, Z.-H.; Xia, X.-H. *Chem. Commun.* **2010**, *46*, 5951−5953.
(19) Yang, Z.; Yao, Z.; Li, G.; Fang, G.; Nie, H.; Liu, Z.; Zhou, X.; Chen, X.; Huang, S. *ACS Nano* **2012**, *6*, 205−211.
(20) Zhang, L.; Xia, Z. *J. Phys. Chem. C* **2011**, *115*, 11170−11176.
(21) Lim, D.; Wilcox, J. *J. Phys. Chem.* **2011**, *115*, 22742−22747.
(22) Krasheninnikov, A. V.; Lehtinen, P. O.; Foster, A. S.; Pyykkö, P.; Nieminen, R. M. *Phys. Rev. Lett.* **2009**, *102*, 126807.
(23) Cretu, O.; Krasheninnikov, A. V.; Rodriguez-Manzo, J. A.; Sun, L.; Nieminen, R.; Banhart, F. *Phys. Rev. Lett.* **2010**, *105*, 196102.
(24) Gong, K.; Du, F.; Xia, Z.; Durstock, M.; Dai, L. *Science* **2009**, *323*, 760.
(25) Chen, Z.; Higgins, D.; Tao, H.; Hsu, R.; Chen, Z. *J. Phys. Chem. C* **2009**, *113*, 21008−21013.
(26) Qu, L.; Liu, Y.; Baek, J.; Dai, L. *ACS Nano* **2010**, *4*, 1321−1326.
(27) Nørskov, J. K.; Bligaard, T.; Rossmeisl, J.; Christensen, C. H. *Nat. Chem.* **2009**, *1*, 37−46.
(28) Banhart, F.; Kotakoski, J.; Krasheninnikov, A. V. *ACS Nano* **2011**, *5*, 26−41.
(29) Krasheninnikov, A. V.; Banhart, F. *Nat. Mater.* **2007**, *6*, 723−733.
(30) Krasheninnikov, A. V.; Nordlund, K. *J. Appl. Phys.* **2010**, *107*, 071301.
(31) Downs, R.; Hall-Wallace, M. *Am. Mineral.* **2003**, *88*, 247−250.
(32) Haynes, W. *CRC handbook of chemistry and physics*; CRC Press: Boca Raton, FL, 2010.
(33) Abraham, M. H. *J. Am. Chem. Soc.* **1982**, *104*, 2085−2094.
(34) Liu, Y.; Sun, H. *J. Comput. Chem.* **2011**, *32*, 1279−1285.
(35) Sha, Y.; Yu, T.; Liu, Y.; Merinov, B.; Goddard, W. A., III *J. Phys. Chem. Lett.* **2010**, *1*, 856−861.
(36) Wilhelm, E.; Battino, R. *Chem. Rev.* **1973**, *73*, 1−9.
(37) Varma, C.; Wilson, A. *Phys. Rev. B* **1980**, *22*, 3795.
(38) Garca-Lastra, J. M.; Mowbray, D. J.; Thygesen, K. S.; Rubio, A.; Jacobsen, K. W. *Phys. Rev. B* **2010**, *81*, 245429.
(39) Lehtinen, O.; Kotakoski, J.; Krasheninnikov, A. V.; Tolvanen, A.; Nordlund, K.; Keinonen, J. *Phys. Rev. B* **2010**, *81*, 153401.
(40) Krasheninnikov, A. V.; Lehtinen, P. O.; Foster, A. S.; Nieminen, R. M. *Chem. Phys. Lett.* **2006**, *418*, 132−136.
(41) Rodriguez-Manzo, J. A.; Cretu, O.; Banhart, F. *ACS Nano* **2010**, *4*, 3422−3428.
(42) Wang, H.; Wang, Q.; Cheng, Y.; Li, K.; Yao, Y.; Zhang, Q.; Dong, C.; Wang, P.; Schwingenschlo, U.; Yang, W.; Zhang, X. X. *Nano Lett.* **2012**, *12*, 141−144.
(43) Kresse, G.; Furthmuller, J. *Comput. Mater. Sci.* **1996**, *6*, 15−50.
(44) Hafner, J. *J. Comput. Chem.* **2008**, *29*, 2044−2078.
(45) Tang, W.; Sanville, E.; Henkelman, G. *J.Phys.: Condens. Matter* **2009**, *21*, 084204.
(46) Kresse, G.; Joubert, D. *Phys. Rev. B* **1999**, *59*, 1758.
(47) Perdew, J. P.; Chevary, J. A.; Vosko, S. H.; Jackson, K. A.; Pederson, M. R.; Singh, D. J.; Fiolhais, C. *Phys. Rev. B* **1992**, *46*, 6671−6687.